Voltage Stability and Control of Offshore Wind Farms With AC Collection and HVDC Transmission

Hanchao Liu, *Student Member, IEEE*, and Jian Sun, *Senior Member, IEEE*

***Abstract*— This paper investigates the stability and control of offshore wind farms employing medium-voltage ac collection and high-voltage dc (HVDC) transmission to the onshore power grids. Type-IV (full power conversion) turbines and HVDC rectifier based on voltage-source converters are assumed. Output impedance models of the wind turbines and input impedance models of the HVDC rectifier in the positive- and negative-sequence are developed using the harmonic linearization method. An impedance-based stability criterion is then applied to determine the stability of the offshore ac collection bus. Possible instability of the ac bus voltage and resonance between the wind farm and the HVDC rectifier are examined through analysis of the system impedance model. The analytical impedance models are used to identify the root causes of such instability and resonance problems, and to develop possible solutions. Detailed circuit simulation is used to validate the analysis. Individual converter impedance models are also validated by experimental measurements of scaled-down prototypes.**

***Index Terms*— Control instability, high-voltage dc (HVDC) transmission, impedance analysis, impedance modeling, offshore wind farms, resonance.**

I. Introduction

HIGH-VOLTAGE dc (HVDC) transmission is attractive for large offshore wind farms that are located far from the onshore power grid [1]. Conventional HVDC technology based on line-commutated converters (LCCs) requires reactive power and voltage support for the offshore ac bus by either a dedicated static synchronous compensator, which significantly increases the overall cost, or through control of individual turbine inverters, which is technically challenging. New HVDC technology based on voltage-source converters (VSCs), including modular multilevel converters [2], avoids the need for reactive power support and also has the ability to black start the system [3]. These make VSC-based HVDC technology the natural choice for offshore wind applications.

Control of conventional LCC-based HVDC converters is slow, with bandwidth limited by phase control and usually well below the fundamental frequency. As a result, stability analysis of traditional HVDC systems can be performed using phasor-based models that are valid below the fundamental frequency [4]. VSC-based HVDC, on the other hand, requires voltage and current control bandwidths that are at least several times of the fundamental frequency to avoid low-order harmonics. Such high-frequency control introduces complex dynamics above the fundamental frequency, thereby creating potentials for new high-frequency instability and resonance problems that are not present in conventional HVDC systems. The same applies to the control of wind turbine converters. Since phasor-based models are invalid above the fundamental frequency, new mathematical models are needed for studying the fast dynamics and high-frequency instability problems in VSC-based HVDC systems. Previous work, e.g. [5] and [6] on offshore wind farm stability failed to recognize this limitation.

Another limitation of the conventional phasor-based analysis method is that it requires design details of individual components of the entire system to formulate a system model, typically in the state-space form [4]. Offshore wind farms with HVDC transmission typically involve multiple suppliers of turbines and HVDC converters as well cables, transformers, protection, and so on. The proprietary nature of the designs of each of these components makes it virtually impossible for suppliers to share the design details required by system modeling and analysis. Numerical simulation [7] has similar limitations, in addition to the fact that it lacks the insight of analytical models and can be difficult to perform due to complexity of the system.

The impedance-based stability analysis method developed in [8] overcomes the limitations of the state-space approach by requiring only the impedance models of each component at the input or output terminal. By applying proper modeling method, such as harmonic linearization [9], impedance models valid both below and above the fundamental frequency can be developed, thereby overcoming the other limitations of phasor-based models. The method was applied in [10] to characterize control instability and high-frequency resonance problems involving single-phase solar inverters. For three-phase converters and systems, the impedance-based stability theory is further extended based on symmetrical components analysis by decomposing the system into a positive-sequence subsystem and a negative-sequence subsystem, and applying the Nyquist-based stability criterion to each subsystem independently [8]. The method has been applied to three-phase inverters connected to the grid [11] as well as LCC HVDC converter systems [12]. Online identification of grid impedance using grid-connected inverters as measurement

Manuscript received February 4, 2014; revised August 3, 2014; accepted August 28, 2014. Date of publication October 1, 2014; date of current version October 29, 2014. This work was supported in part by the Stanford Global Climate and Energy Program and in part by the National Science Foundation under Award ECCS-1002265. Recommended for publication by Associate Editor Frans Dijkhuizen.

The authors are with the Department of Electrical, Computer, and Systems Engineering, Rensselaer Polytechnic Institute, Troy, NY 12180 USA (e-mail: liuh9@rpi.edu; jsun@rpi.edu).

Color versions of one or more of the figures in this paper are available online at http://ieeexplore.ieee.org.

Digital Object Identifier 10.1109/JESTPE.2014.2361290

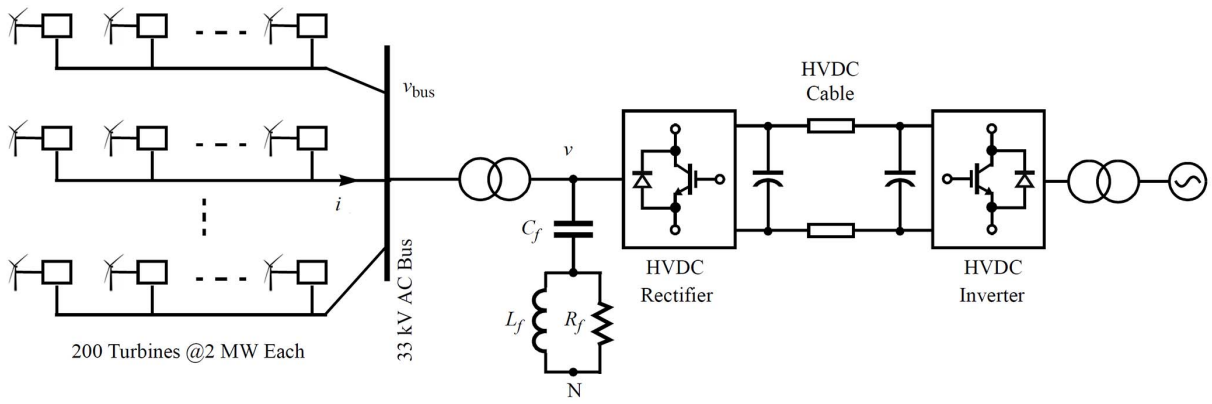

Fig. 1. Single-line diagram of an offshore wind farm with VSC-based HVDC transmission.

devices has also been proposed [13] to enable adaptive control [14].

This paper uses the impedance-based modeling and analysis method reviewed above to study stability and resonance problems in offshore wind farms with HVDC transmission. A single-line diagram of the studied system is given in Fig. 1. It will be demonstrated that control instability and resonance both below and above the ac bus fundamental frequency may occur in this type of system and that these problems can be predicted from system impedance analysis and effectively mitigated through control design changes based on the impedance models. The rest of this paper is organized as follows. Section II provides the details of the system studied and small-signal impedance models of the wind inverter as well as of the HVDC rectifier. Section III presents stability analysis of the system using the impedance-based method. Different behaviors of the system are characterized and verified by detailed time-domain circuit simulation. Section IV demonstrates the use of the analytical impedance models in the design of turbine inverter as well as HVDC rectifier control to mitigate system instability and resonance problems. Section V concludes this paper.

II. System Description and Modeling

A. Offshore Wind Farm With HVDC Transmission

Refer to Fig. 1 for a single-line diagram of the offshore wind farm with HVDC transmission system studied in this paper. It is assumed that the wind farm consists of 200 wind turbines, each employing a permanent-magnet synchronous generator and a back-to-back power conversion system (Type-IV turbines). Each turbine is rated at 2 MW. The nominal ac collection bus voltage is 33 kV, which is stepped up to 150 kV for feeding into the HVDC rectifier. The offshore rectifier station is assumed to be 150 km away from the onshore inverter station. Standard two-level VSC is assumed for the wind turbine rectifier and inverter as well as the HVDC rectifier and inverter.

Fig. 2 shows a simplified diagram of the wind inverter and its control. Each turbine inverter is controlled as a current source to inject active power to the ac bus. While the inverter can also supply reactive power and participate in ac bus

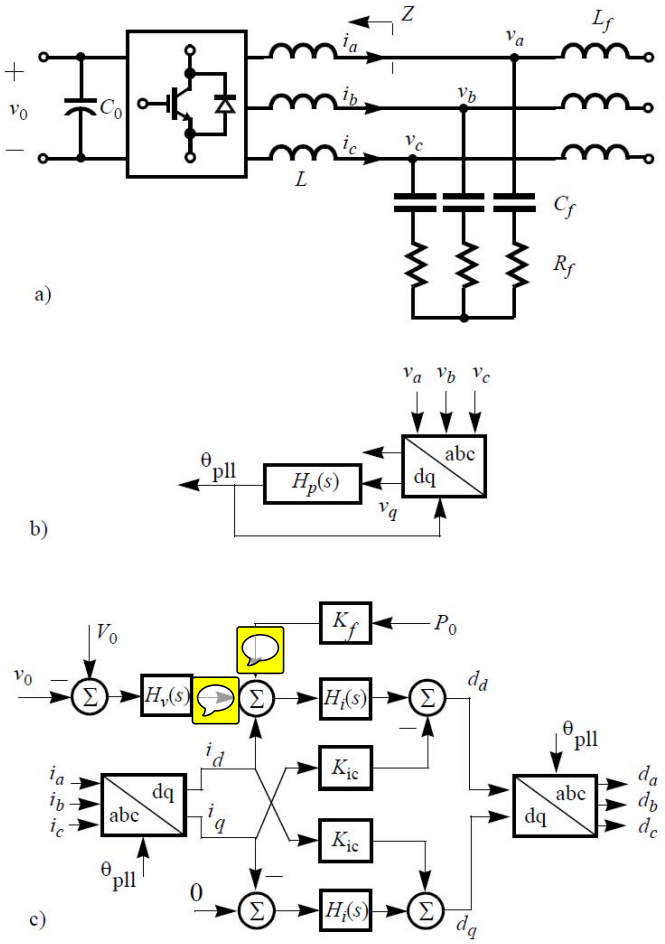

Fig. 2. Wind inverter and its control. (a) Simplified circuit diagram. (b) PLL. (c) DC link voltage and ac current control.

voltage regulation, such capabilities are currently not considered in this paper. A phase-locked loop (PLL) is used to synchronize the inverter current to the ac bus voltage. A dq-frame current control scheme is used and the current reference is provided by the dc link voltage regulator. The current compensator transfer function is given by

$$H_i(s) = K_p + \frac{K_i}{s} \tag{1}$$

TABLE I
CIRCUIT AND CONTROL PARAMETERS OF WIND INVERTER

Parameter	Symbol	Value
Dc Bus Voltage	V_0	1500 V
Phase Voltage Amplitude	V_1	563 V
Phase Current Amplitude	I_1	236 kA
Phase Inductance	L	0.526 μH
Output Filter Inductance	L_f	0.5 μH
Output Filter Capacitance	C_f	0.207 F
Output Filter Damping Resistance	R_f	2.75 mΩ
Current Control Compensator $H_i(s)$	K_p	0.44×10^{-6}
	K_i	0.55×10^{-3}
Current Decoupling Coefficient	K_{id}	22.5×10^{-6}
Current Control Bandwidth	f_i	250 Hz
PLL Compensator $H_p(s)$	K_p	0.239
	K_i	45
PLL Bandwidth	f_{pll}	30 Hz

and the PLL is implemented using a PI regulator in the *dq* reference frame [16]. Including the integrator to convert the frequency into angle, the overall PLL compensation function is

$$H_p(s) = \left(K_p + \frac{K_i}{s}\right)\frac{1}{s}. \tag{2}$$

To simplify the analysis, the 200 turbines are lumped into two units each rated at 200 MW. The equivalent 200-MW turbine circuit and control parameters are provided in Table I. The rectifier at each turbine is controlled using standard torque and speed control methods [16] to extract the maximum power from the turbine. Since the dynamics of the rectifier and generator are decoupled from the ac bus voltage by the large dc link capacitor, they are not considered in the small-signal analysis. Hence, the details of the rectifier control are omitted here.

The HVDC rectifier is controlled to behave as a voltage source at the ac terminals [15]. The HVDC link voltage is regulated by the onshore inverter while the offshore HVDC rectifier injects current to it. Under normal operation, each turbine operates at its maximum power point and the HVDC rectifier transmits all power to the HVDC link. The frequency of the ac collection bus is set by the HVDC rectifier using an internal reference. This frequency reference can be adjusted to send a signal to wind turbines for power curtailment when, e.g., the onshore inverter station cannot accept all the power transmitted. The HVDC rectifier voltage control is performed by a PI regulator in the *dq* reference frame

$$H_v(s) = K_p + \frac{K_i}{s}. \tag{3}$$

A current loop is embedded within the voltage loop, and the current compensator transfer function is defined as

$$H_i(s) = K_p + \frac{K_i}{s}. \tag{4}$$

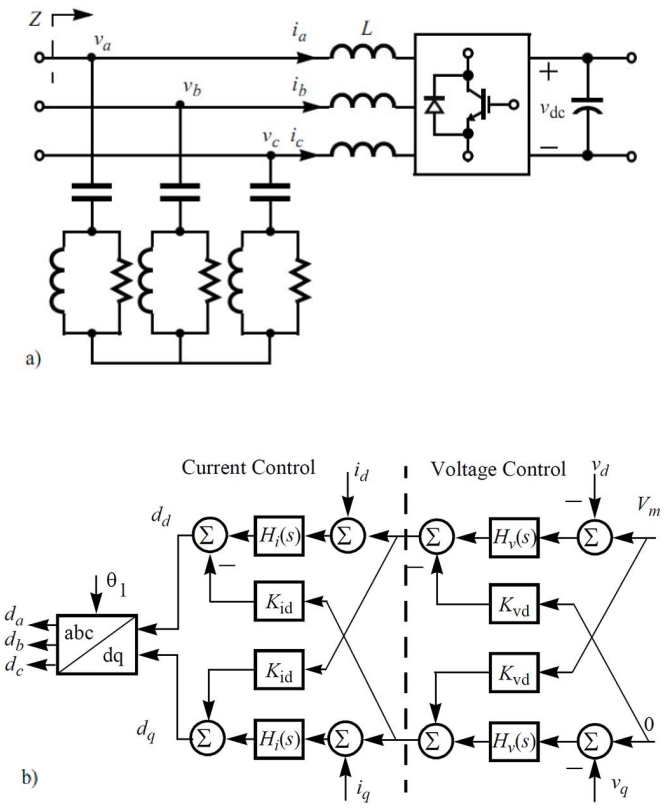

Fig. 3. HVDC rectifier and control. (a) Simplified circuit diagram. (b) AC bus voltage control with an embedded current control loop.

Current feedforward control can also be incorporated to improve the voltage regulation but is not considered in this paper. Fig. 3 shows the circuit and control diagrams of the offshore HVDC rectifier, with their parameters provided in Table II.

B. Small-Signal Impedance Modeling

The output impedance model of each wind turbine inverter and the input impedance model of the HVDC rectifier can be developed using the harmonic linearization method described in [17]. In general, each converter can be described by a positive-sequence impedance and negative-sequence impedance without cross coupling [11].

In modeling the wind inverter output impedance, the dc bus voltage is assumed to be constant such that dynamics of the voltage control loop and the turbine rectifier can be ignored. This assumption is valid above the bandwidth of the dc bus voltage control, which is typically limited to the 10-Hz range. The resulting turbine inverter output impedance models are given by

$$Z_p(s) = \frac{H_i(s - j\omega_1)V_0 + (s - j\omega_1)L}{1 - T_{\text{pll}}(s - j\omega_1)[1 + H_i(s - j\omega_1)I_1V_0/V_1]} \tag{5}$$

$$Z_n(s) = \frac{H_i(s + j\omega_1)V_0 + (s + j\omega_1)L}{1 - T_{\text{pll}}(s + j\omega_1)[1 + H_i(s + j\omega_1)I_1V_0/V_1]} \tag{6}$$

where the subscript p denotes the positive sequence and n the negative sequence. Here, $T_{\text{pll}}(s)$ is the loop gain of the

TABLE II
CIRCUIT AND CONTROL PARAMETERS OF HVDC RECTIFIER

Parameter	Symbol	Value
HVDC Dc Link Voltage	V_{dc}	300 kV
Phase Voltage Amplitude	V_m	122 kV
Phase Inductance	L	17.9 mH
Ac Filter Inductance	L_f	0.43 μH
Ac Filter Capacitance	C_f	17.7 μF
Ac Filter Resistance	R_f	10 Ω
Current Control Compensator $H_i(s)$	K_p	0.075×10^{-3}
	K_i	0.094
Current Decoupling Coefficient	K_{id}	23×10^{-6}
Current Control Bandwidth	f_i	250 Hz
Voltage Control Compensator $H_v(s)$	K_p	11.1×10^{-3}
	K_i	8.388
Voltage Decoupling Coefficient	K_{vd}	5.56×10^{-3}
Voltage Control Bandwidth	f_v	100 Hz

dq-frame PLL defined by

$$T_{pll}(s) = \frac{V_1 H_p(s)}{2[1 + V_1 H_p(s)]} \tag{7}$$

and $H_i(s)$ and $H_p(s)$ are the current and PLL compensator transfer functions, respectively, as defined before. ω_1 is the fundamental angular frequency (120 π rad/s). Other variables have been defined in Table I. Note that (5) and (6) define the output impedance of the inverter including the ac inductors but excluding the LC filter, as shown in Fig. 2.

The HVDC link voltage is treated as a constant when modeling the input impedance of the HVDC rectifier. This assumption is again justified on the basis of the large dc capacitance and the slow dynamics of the HVDC dc link voltage. The resulting positive-sequence and negative-sequence input impedance models of the HVDC rectifier are

$$Z_p(s) = \frac{H_i(s - j\omega_1)V_{dc} + sL}{1 + Y(s)[H_i(s - j\omega_1)V_{dc} + sL] + T_p(s)} \tag{8}$$

$$Z_n(s) = \frac{H_i(s + j\omega_1)V_{dc} + sL}{1 + Y(s)[H_i(s + j\omega_1)V_{dc} + sL] + T_n(s)} \tag{9}$$

where $H_i(s)$ and $H_v(s)$ are the current and voltage compensator transfer functions defined before, $Y(s)$ is admittance of the ac filter, and $T_p(s)$ and $T_n(s)$ are defined as

$$T_p(s) = [H_i(s - j\omega_1) + jK_{id}]H_v(s - j\omega_1)V_{dc} \tag{10}$$

$$T_n(s) = [H_i(s + j\omega_1) - jK_{id}]H_v(s + j\omega_1)V_{dc}. \tag{11}$$

The numerators in (8) and (9) are similar to that in the turbine inverter output impedance, indicating that the current control effectively adds a series element to the VSC input impedance. But unlike the turbine inverter output impedance that changes with the ac bus voltage and current, the HVDC rectifier input impedance is independent of the operation conditions, due to the fact that it does not involve a PLL.

TABLE III
CIRCUIT PARAMETERS OF THE PROTOTYPE

	Parameter	Symbol	Value
Inverter	Dc Bus Voltage	V_0	400 V
	Phase Voltage Amplitude	V_1	170 V
	Rated Power	P	5 kW
	Phase Inductance	L	3.4 mH
	Switching Frequency	f_s	20 kHz
Rectifier	Dc Bus Voltage	V_{dc}	200 V
	Phase Voltage Amplitude	V_m	90 V
	Rated Power	P	5 kW
	Phase Inductance	L	3.1 mH
	Ac Filter Capacitance	C_f	22 μF
	Ac Filter Resistance	R_f	1.3 Ω
	Switching Frequency	f_s	20 kHz

TABLE IV
CONTROL PARAMETERS OF THE PROTOTYPE

Control Parameter	Value
Inverter Current Control (K_p, K_i)	(0.047, 148)
Inverter PLL (K_p, K_i)	(0.269, 16.42)
Rectifier Current Control (K_p, K_i)	(0.075, 50)
Rectifier Voltage Control (K_p, K_i)	(0.0019, 0.48)

To provide a validation of these impedance models, two scaled-down VSC modules have been used to emulate the wind inverter and the HVDC rectifier. In each case, the control functions defined above were implemented and the impedance responses of the converter were then measured using the setup described in [18]. Table III summarizes the parameters of the scaled-down hardware. Because of the different switching frequency and other circuit parameters, the control parameters are also adjusted from those of the original wind inverter and HVDC rectifier design, as listed in Table IV.

Figs. 4 and 5 compare the measured impedance responses with those predicted by the analytical models (5), (6), (8), and (9). The measurements agree with the model prediction except for a narrow frequency range around the fundamental frequency (60 Hz) in which the impedance cannot be reliably measured due to the difficulties for the measurement instruments to distinguish the fundamental voltage from the injected perturbation.

III. SYSTEM BEHAVIOR AND SMALL-SIGNAL ANALYSIS

The offshore wind farm system as described in the previous section was implemented in Saber [19] using detailed ideal switch models. Operation of the system under different control designs and operation conditions was then simulated. Two representative cases are presented below to highlight possible ac bus voltage instability and resonance problems.

Fig. 6 shows the simulated responses of the ac bus voltages and wind inverter output currents when the wind farm is producing 60% of its rated (400 MW) power. It can be observed

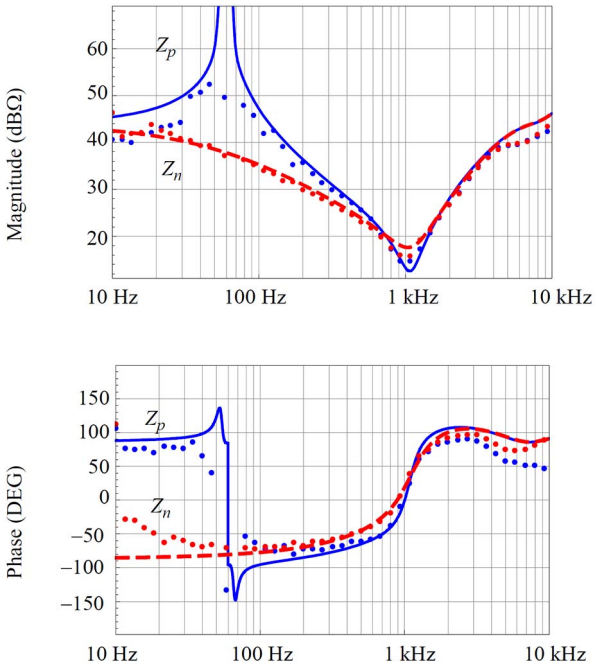

Fig. 4. Validation of wind inverter output impedance models by measurement from a scaled-down hardware prototype. Solid lines: positive sequence. Dashed lines: negative sequence. Dots: measurements.

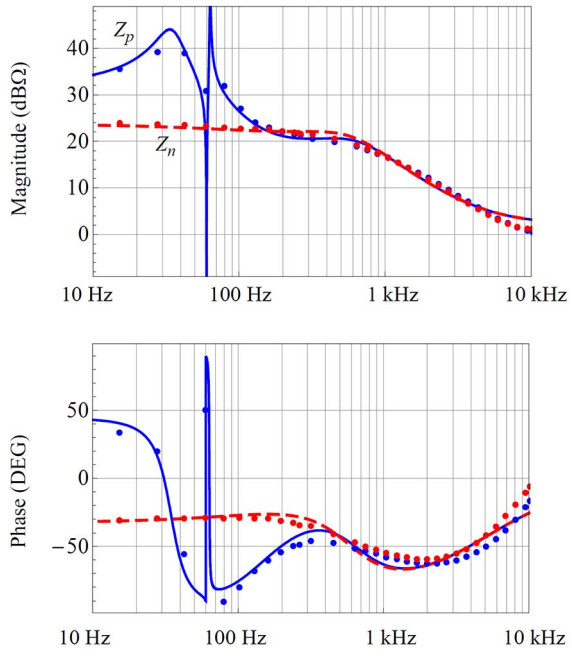

Fig. 5. Validation of HVDC rectifier input impedance model by measurement from a scaled-down hardware prototype. Solid lines: positive sequence. Dashed lines: negative sequence. Dots: measurements.

that the amplitude of both voltages and currents oscillates at 30 Hz. In the spectra of the voltage and current, this amplitude modulation appears as harmonics at 30 and 90 Hz. The system becomes unstable, with currents and voltages running away, if the transferred power is increased beyond 60% rated power.

The second case simulated involves a modified HVDC rectifier ac filter design. To see the effects of filter on ac bus voltage stability, the design was modified to use less

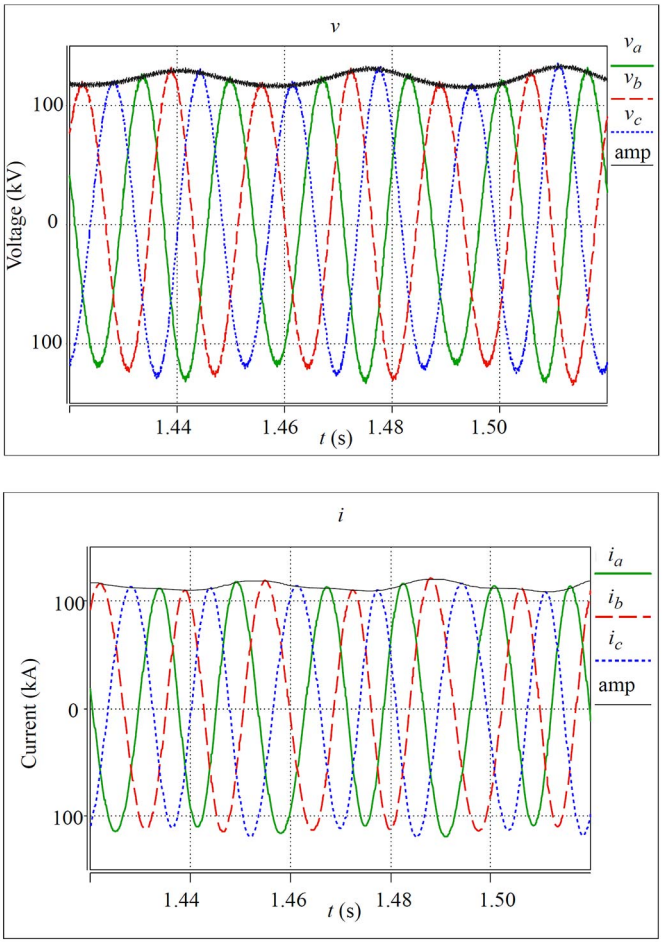

Fig. 6. Simulated responses of ac collection bus voltage (upper) and currents (lower) with 30-Hz amplitude modulation.

capacitance ($C_f = 3.52\ \mu$F) while the inductance is increased to 1.72 mH to preserve filter attenuation. Meanwhile, the wind inverter PLL bandwidth is increased to 90 Hz, and its current control bandwidth is increased to 800 Hz. In addition, the wind inverter filter inductance L_f is reduced to 0.125 μH.

Fig. 7 shows the resulting responses of the ac bus voltages and turbine inverter output currents when the wind farm operates at 60% of its rated power. A resonance above the ac bus fundamental frequency (supersynchronous resonance [20]) can be observed. Fourier analysis indicated the resonant frequency is 210 Hz. The nonharmonic resonance causes the current and voltage waveforms to change from cycle to cycle.

The impedance-based system analysis method presented in [8] can be applied to understand the resonance behavior and to find the root causes. For that purpose, Fig. 8 shows the small-signal representation of the ac collection bus system where $Z_w(s)$ represents the output impedance of the lumped wind turbines including the impedance of the turbine inverter output filter, $Z_r(s)$ is the input impedance of the HVDC rectifier including its input filter, and $Z_c(s)$ is the impedance of the 33 kV cable between the turbines and the transformer. All impedances are measured at the 33 kV bus and the low-voltage (33 kV) side of the transformer is considered the point of common coupling (PCC) for the wind farm. The transformer

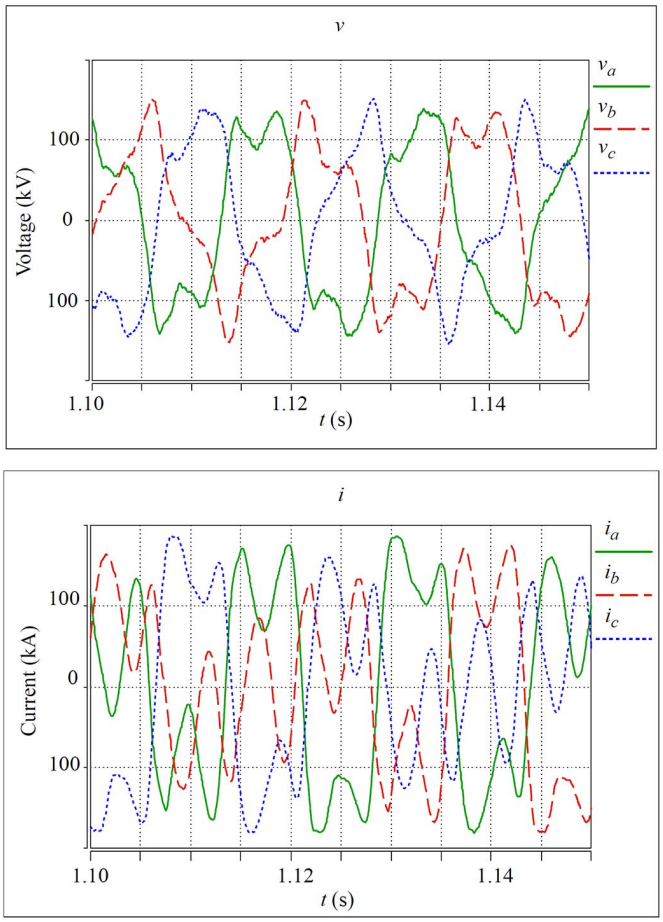

Fig. 7. Simulated responses of ac collection bus voltage (upper) and currents (lower) with supersynchronous resonance.

is assumed ideal in this study; the reactance of a non-ideal transformer can be modeled as part of the input impedance of the HVDC rectifier. The same form of equivalent circuit can be used for both the positive-sequence and negative-sequence impedance. To apply the stability theory presented in [8], the system is partitioned at the PCC defined above: The HVDC rectifier acts as the "grid" for the wind farm and $Z_r(s)$ is the equivalent grid impedance. Based on the theory presented in [8], the system is stable if and only if the impedance ratio

$$\frac{Z_r(s)}{Z_w(s)+Z_c(s)} \tag{12}$$

satisfies the Nyquist criterion for both the positive and negative sequence impedances. Resonance occurs in either sequence when the corresponding sequence impedance ratio satisfies the Nyquist criterion but doesn't have sufficient stability margin [8, 10, 11].

The underlying assumptions for the system partition which (12) is based on are that

1) The HVDC rectifier control is stable and well behaved before the wind farm is connected to the PCC; and
2) the wind turbine control is designed such that the wind farm, including the medium-voltage cable network, is stable and well behaved when connected to an ideal grid at the PCC.

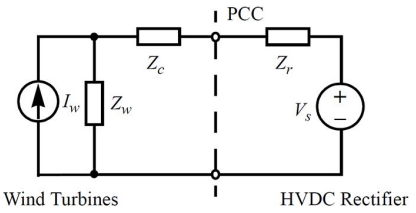

Fig. 8. Impedance model of the offshore ac grid system.

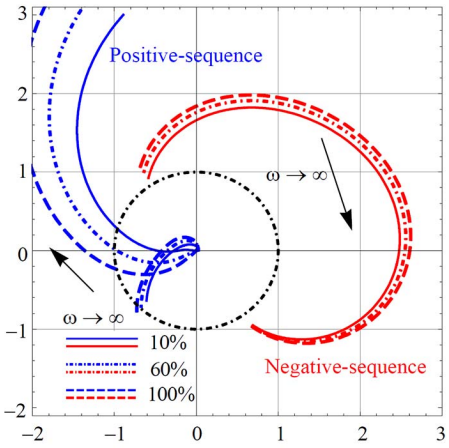

Fig. 9. Nyquist responses of the system impedance ratio for simulated case shown in Fig. 6. Additional responses for 10% and 100% rated power are also provided.

The first assumption is trivial and represents a common design practice and minimal requirement for the HVDC rectifier. The second assumption requires turbine control design to consider the cable impedance between the turbine and the PCC. Since the characteristics of this cable are usually known to the turbine designer and the cable is usually short, it is reasonable to assume that the turbine control remains stable and well behaved in the presence of the cable either by considering the cable impedance in the design or by virtue of robustness of control design. In the case that the wind farm spreads over a large area with complex cable connections that may cause instability and resonance within the farm itself, a separate analysis should be conducted first by assuming an ideal grid behind the PCC before applying the above partition to assess instability and resonance between the wind farm and the HVDC rectifier [11].

For the first case simulated above, Fig. 9 shows the Nyquist plot of the impedance ratio defined by (12) in the positive and negative sequence. In addition to the simulated case when the system operates with 60% rated power, two additional cases with 10% and 100% rated power are also provided for comparison. As can be seen, the positive-sequence impedance ratio moves toward the $(-1, 0)$ point as the power level increases. At 60% rated power, the impedance ratio intersects with the unit circle at 90 Hz, with a phase margin of about 3°. The lack of phase margin explained the observed resonance at 90 Hz. The Nyquist plot also indicates that the negative-sequence impedance ratio does not intersect with the unit circle, hence has no stability problem in the negative

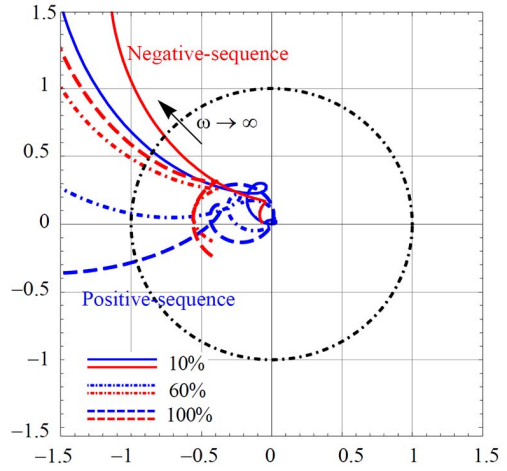

Fig. 10. Nyquist responses of the system impedance ratio for simulated case shown in Fig. 7. Additional responses for 10% and 100% rated power are also provided.

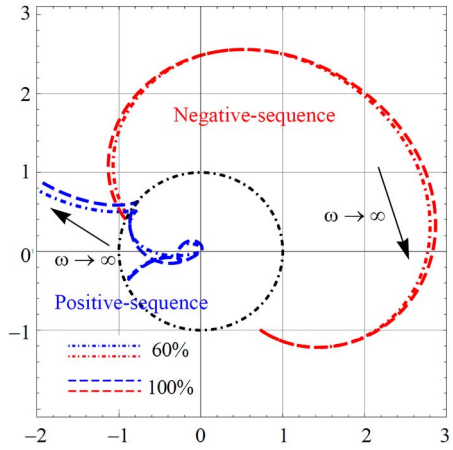

Fig. 11. Nyquist responses of the system impedance ratio when a PR regulator is added to the HVDC rectifier voltage control for 60% and 100% rated power.

sequence. The Nyquist plot further indicates that the system will operate well at 10% rated power but will lose stability entirely at 100% rated power, which has been confirmed by detailed circuit simulation.

Fig. 10 shows similar responses for the second simulated case presented in Fig. 7. At 60% rated power, the Nyquist plot intersects with the unit circle at around 210 Hz in this case, with a phase margin of 5°. The lack of phase margin leads to the supersynchronous resonance at 210 Hz observed in Fig. 7. The Nyquist plots also indicate that the system cannot operate stably at 100% rated power, but will not have any stability or resonance problem at 10% rated power. These have also been confirmed by detailed circuit simulation.

IV. System Stabilization by Control Modification

The impedance models presented in Section II not only provide a means to characterize the behavior of the system but also to solve instability and resonance problems. Specifically, the analytical form of the impedance models makes it possible to identify key circuit and control parameters that affect the impedance behavior of each converter near the intersection frequency of the impedance ratio with the unit circle and to determine possible ways to increase the phase margin. We will demonstrate this using the first simulated case (with subsynchronous resonance) presented in the previous section.

A. Changing HVDC Rectifier Control

The HVDC rectifier input impedance models (8) and (9) indicate that faster voltage control helps lower the input impedance, thereby reducing the potential for instability and resonance. The voltage loop was originally designed to have 100-Hz crossover frequency with 60° phase margin. By changing the voltage compensator proportional gain (K_p) to 14.81×10^{-3} and the integral gain (K_i) to 14.9, the voltage loop crossover frequency is increased to 150 Hz, with 60° phase margin. Numerical simulation shows that the system can operate stably without resonance up to 100% rated power.

The HVDC rectifier control bandwidth is limited by the switching frequency and increasing it may not be practical. As an alternative, the input impedance may also be reshaped by adding to the voltage compensator a proportional resonant (PR) gain block

$$k_p + \frac{k_i s}{s^2 + k_d s + \omega^2} \tag{13}$$

where $k_p = 1$, $k_i = 100$, $k_d = 100$, and $\omega = 2\pi \times 44$. The added PR compensator reduces the rectifier input impedance near 16 and 104 Hz while keeping the impedance at other frequencies unchanged.

Fig. 11 shows the Nyquist plots of the impedance ratio (12) with such a PR voltage compensator. As can be seen, there is 45° phase margin even under 100% rated power. To demonstrate the effects of the added PR compensation, Fig. 12 shows the simulated system responses when the transferred power is increased from 80% to 100% rated power at $t = 1.2$ s.

It has also been observed that slower inner current loop of HVDC rectifier helps to reduce the input impedance, thereby improving system stability. However, slower current loop results in poor voltage transient and is also undesirable for system operation under fault. Another option is to remove the current loop entirely. The analytical impedance models (8) and (9) can be adopted to study the effects on system stability. The details are omitted here due to space limit.

B. Changing Wind Turbine Inverter PLL Design

The wind turbine inverter output impedance models (5) and (6) indicate that current control and PLL design have significant effects on the impedance, hence also system stability. To demonstrate the effects, the PLL is redesigned to reduce its bandwidth to 15 Hz by changing its compensator parameters proportional gain (K_p) to 0.12 and the integral gain (K_i) to 11.3. Fig. 13 shows the resulting Nyquist plot of the system impedance ratio (12), which indicates that the system is stable even at 100% rated power, with a phase margin of 35°.

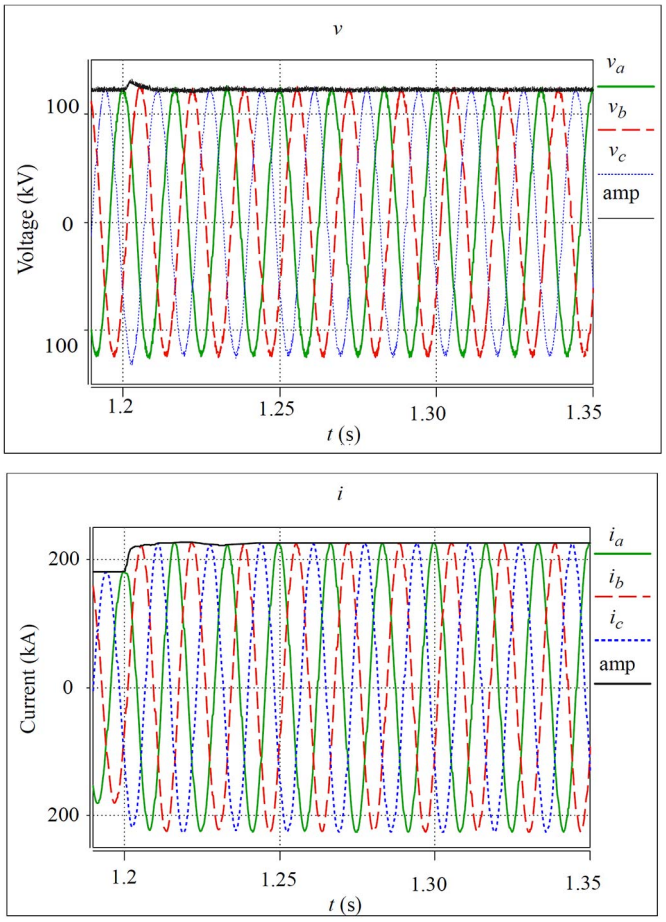

Fig. 12. Simulated responses of ac collection bus voltage (upper) and currents (lower) when HVDC rectifier voltage control includes a PR compensator.

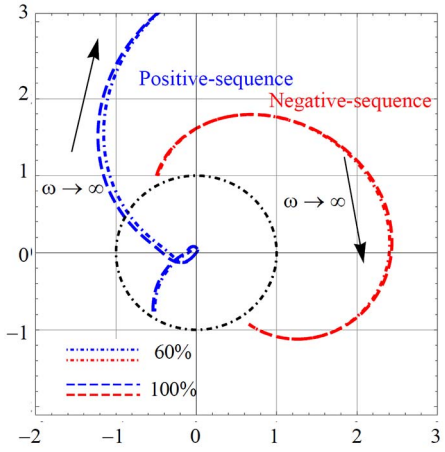

Fig. 13. Nyquist responses of the system impedance ratio when a slow PLL is used at the wind inverter for 60% and 100% ratios.

Note that the PLL bandwidth needs to be selected also in consideration of other performances of the wind turbine inverter control [16]. On the other hand, many of the considerations for wind turbines connected directly to the power grid may not be applicable for offshore wind farms. Therefore, PLL design, or even the use of PLL in offshore wind farms with HVDC transmission should be reconsidered and will be the subject of future work.

V. Conclusion

Voltage stability and control in offshore wind farms with HVDC transmission have been studied in this paper. It was demonstrated by detailed circuit simulation that instability as well as resonance both below and above the synchronous frequency may occur. An impedance-based system model was presented, and the Nyquist stability criterion was applied to the ratio of the HVDC rectifier input impedance to the wind farm output impedance to determine system stability. Resonance was shown to originate from the lack of stability margin of the said impedance ratio in either the positive or the negative sequence. The analytical impedance models also provided a basis for circuit and control design modification to mitigate possible instability and resonance problems. In particular, the effects of wind inverter current control and PLL design as well as the HVDC rectifier voltage and current control on system dynamics and stability were studied using the impedance models. Stabilization of the ac collection bus voltage and the elimination of resonance through modification of these control functions have been demonstrated.

References

[1] N. M. Kirby, L. Xu, M. Luckett, and W. Siepmann, "HVDC transmission for large offshore wind farms," *Power Eng. J.*, vol. 16, no. 3, pp. 135–141, Jun. 2002.

[2] M. Saeedifard and R. Iravani, "Dynamic performance of a modular multilevel back-to-back HVDC system," *IEEE Trans. Power Del.*, vol. 25, no. 4, pp. 2903–2912, Oct. 2010.

[3] G. P. Adam, K. H. Ahmed, S. J. Finney, K. Bell, and B. W. Williams, "New breed of network fault-tolerant voltage-source-converter HVDC transmission system," *IEEE Trans. Power Syst.*, vol. 28, no. 1, pp. 335–346, Feb. 2013.

[4] P. Kundur, *Power System Stability and Control*. New York, NY, USA: McGraw-Hill, 1994.

[5] L. Wang and K.-H. Wang, "Dynamic stability analysis of a DFIG-based offshore wind farm connected to a power grid through an HVDC link," *IEEE Trans. Power Syst.*, vol. 26, no. 3, pp. 1501–1510, Aug. 2011.

[6] L. Wang and M. S. N. Thi, "Comparative stability analysis of offshore wind and marine-current farms feeding into a power grid using HVDC links and HVAC line," *IEEE Trans. Power Del.*, vol. 28, no. 4, pp. 2162–2171, Oct. 2013.

[7] A. de la Villa Jaen, E. Acha, and A. G. Exposito, "Voltage source converter modeling for power system state estimation: STATCOM and VSC-HVDC," *IEEE Trans. Power Syst.*, vol. 23, no. 4, pp. 1552–1559, Nov. 2008.

[8] J. Sun, "Impedance-based stability criterion for grid-connected inverters," *IEEE Trans. Power Electron.*, vol. 26, no. 11, pp. 3075–3078, Nov. 2011.

[9] J. Sun, "Small-signal methods for AC distributed power systems—A review," *IEEE Trans. Power Electron.*, vol. 24, no. 11, pp. 2545–2554, Nov. 2009.

[10] X. Chen and J. Sun, "A study of renewable energy system harmonic resonance based on a DG test-bed," in *Proc. 26th Annu. IEEE Appl. Power Electron. Conf. Expo.*, Mar. 2011, pp. 995–1002.

[11] M. Cespedes and J. Sun, "Impedance modeling and analysis of grid-connected voltage-source converters," *IEEE Trans. Power Electron.*, vol. 29, no. 3, pp. 1254–1261, Mar. 2014.

[12] H. Liu and J. Sun, "Small-signal stability analysis of offshore wind farms with LCC HVDC," in *Proc. IEEE Grenoble PowerTech*, Jun. 2013, pp. 1–8.

[13] T. Roinila, M. Vilkko, and J. Sun, "Online grid impedance measurement using discrete-interval binary sequence injection," in *Proc. IEEE 14th Workshop Control Modeling Power Electron.*, Jun. 2013, pp. 1–8.

[14] M. Cespedes and J. Sun, "Adaptive control of grid-connected inverters based on online grid impedance measurements," *IEEE Trans. Sustainable Energy*, vol. 5, no. 2, pp. 516–523, Apr. 2014.

[15] E. Larsen, G. Drobnjak, and H. Elahi, "Standardization of VSC-HVdc interface with offshore wind generation," in *Proc. 11th Int. Workshop Large-Scale Integr. Wind Power Power Syst.*, Nov. 2012. pp. 169–174

[16] F. Blaabjerg, R. Teodorescu, M. Liserre, and A. V. Timbus, "Overview of control and grid synchronization for distributed power generation systems," *IEEE Trans. Ind. Electron.*, vol. 53, no. 5, pp. 1398–1409, Oct. 2006.
[17] Z. Bing, K. J. Karimi, and J. Sun, "Input impedance modeling and analysis of line-commutated rectifiers," *IEEE Trans. Power Electron.*, vol. 24, no. 10, pp. 2338–2346, Oct. 2009.
[18] M. Cespedes and J. Sun, "Three-phase impedance measurement for system stability analysis," in *Proc. 14th IEEE Workshop Control Modeling Power Electron.*, Jun. 2013, pp. 1–6.
[19] *Saber Manual*, Synopsys, Inc., Mountain View, CA, USA. [Online]. Available: http://www.synopsys.com/Systems/Saber, accessed 2014.
[20] J. Sun, "Modeling and analysis of supersynchronous resonance by sequence impedances," in *Proc. IEEE Energy Convers. Congr. Expo.*, Sep. 2014.

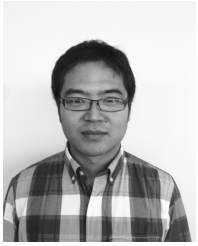

Hanchao Liu (S'12) received the B.S. degree from Shandong University, Jinan, China. He is currently pursuing the Ph.D. degree with the Rensselaer Polytechnic Institute, Troy, NY, USA.

His current research interests include modeling and control of power electronics converters, system stability analysis, and grid integration of renewable energy.

Jian Sun (M'95–SM'09) received the B.S. degree from the Nanjing Institute of Aeronautics, Nanjing, China, the M.S. degree from the Beijing University of Aeronautics and Astronautics, Beijing, China, and the Dr.Ing. (Ph.D.) degree from the University of Paderborn, Paderborn, Germany, all in electrical engineering.

He was a Post-Doctoral Fellow with the School of Electrical and Computer Engineering, Georgia Institute of Technology, Atlanta, GA, USA, from 1996 to 1997. He was with the Advanced Technology Center, Rockwell Collins, Inc., Cedar Rapids, IA, USA, from 1997 to 2002, where he led research on advanced power conversion for aerospace applications. In 2002, he joined the Rensselaer Polytechnic Institute, Troy, NY, USA, where he is currently a Professor and the Director of the New York State Center for Future Energy Systems. He has authored over 170 journal and conference papers, and holds nine U.S. patents. His current research interests include power electronics and energy conversion, with a focus on modeling, control, and applications in aerospace and renewable energy systems.

Dr. Sun is a Senior Member of the IEEE Power Electronics Society. He served as the Editor-in-Chief of the IEEE POWER ELECTRONICS LETTERS from 2008 to 2014. He also served as the Chair of the IEEE Power Electronics Society's Technical Committee on Power and Control Core Technologies until 2012, and became the Treasurer of the IEEE Power Electronics Society (PELS) in 2013. He was the General Chair of the 2006 IEEE Workshop on Computers in Power Electronics, and was involved in the organization of numerous other PELS conferences. He was a recipient of the PELS Modeling and Control Technical Achievements Award in 2013 for contributions to averaged modeling and stability analysis of ac power electronics systems.